The stretched cell cycle model

(Supporting Information Appendix)

Mark R. Dowling[a,b,1], Andrey Kan[a,b,1], Susanne Heinzel[a,b], Jie H. S. Zhou[a,b], Julia M. Marchingo[a,b], Cameron J. Wellard[a,b], John F. Markham[a,b,2] and Philip D. Hodgkin[a,b,2,3]

[a]Division of Immunology, Walter and Eliza Hall Institute of Medical Research, Parkville, VIC 3052, Australia; and [b]Department of Medical Biology, University of Melbourne, Parkville, VIC 3010, Australia; and [c]Victoria Research Laboratory, National ICT Australia, University of Melbourne, Parkville, VIC 3010, Australia

[1]M.R.D. and A.K. contributed equally to this work.

[2]J.F.M. and P.D.H. contributed equally to this work.

[3]To whom correspondence should be addressed. E-mail: hodgkin@wehi.edu.au

SI Text 1

Fitting models to alpha plots. An alpha plot as introduced by Smith and Martin (1) is essentially a survival curve or *1 – cumulative distribution function (CDF)*. Here we consider empirical alpha plots of total division time (T_{div}), duration of S/G_2/M part (T_{grn}), and duration of G_1 phase ($T_{div} - T_{grn}$) from the four experiments. At least for two of the experimental conditions, CpG stimulated B cells and αCD3 and IL-2 stimulated T cells (both harvested after approximately 1 day), cell death can be ignored, and hence the empirical distribution of total division times can be considered to approximate a "true" physiological distribution. For the other two experimental conditions cell death might censor observed division times (2). These potentially censored alpha-curves for total division times can still be approximated reasonably well by the models considered in this section. The emphasis of this section is that the stretched cell cycle model can simultaneously explain distributions of total division times and the duration of G_1 and S/G_2/M phases, whereas the considered transitional probability models do not fit the data for the individual phases well.

When constructing stretched models, we considered a variety of distributions for total division time. We chose lognormal for the fits in Fig. 3 as we have previously found it to provide good fits to division time data (3). However, other right-skewed distributions such as gamma, inverse Gaussian or Weibull can provide equally good fits. Of note, some of the data sets presented here appear more symmetrical than in some of our previous work, so we also considered a normal (Gaussian) distribution for total division time. When fit to data, we found that the normal performed marginally

better than the right-skewed distributions only for the B cell αCD40 data (the reason being that even right-skewed distributions can fit relatively symmetric looking data depending on the choice of parameters). We acknowledge that the best choice of distribution may depend on cell type and stimulation condition, however this was not the main focus here so we chose the same distribution for all. Lognormal provided the best fits overall, and so is shown in Fig. 3. Inverse Gaussian is illustrated in Fig. S5 to make the point that other right-skewed distributions can provide equally good fits. Inverse Gaussian has the interesting interpretation that it is the time taken for a Brownian motion process to pass a fixed threshold, which may provide insight at the molecular level as first suggested by Castor (4). Whatever one's preference for total division time distribution, one can always construct a stretched version by adding "stretching" parameter/s to predict internal cell cycle phases.

We fit the models listed in SI Table S1 to our filming data results. There is a strong correlation in measured times for siblings, and therefore from each experiment we used data only for one randomly chosen sibling (B cells, CpG *N = 49*; B cells, αCD40 *N = 17*; CD8+ T cells *N = 56*; OT-I cells *N = 143*). For simplicity, measurement noise was assumed to be negligible compared to real variation in data.

The choice of fitting strategy depended on the model. For the stretched lognormal and stretched inverse Gaussian models, maximum likelihood estimation (MLE) was used to fit the distribution of total division times. The distributions for the G_1 and $S/G_2/M$ phases were then calculated using the stretching parameters, k_{SG2M} and $k_{G1} = 1 - k_{SG2M}$, extracted from the fits in Fig. 2. For "E.xp. + lag" and "Exp. + Gaussian" models we evaluated two different fitting strategies. For Exp. + lag, the CDF follows a horizontal line for the lag time, t_0, followed by a linear decay when plotted on a log scale. Therefore the simplest fitting strategy (shown in Fig. 3) is to fit a straight line to the empirical CDF. An alternative is to attempt a MLE, however the difficulty is that if $t_0 > min(T_{div})$, the probability is zero. Furthermore, whatever the slope, λ, setting $t_0 = min(T_{div})$ maximises the probability. Therefore we set $t_0 = min(T_{div})$, and use a MLE approach to find the slope, λ. The fit using this approach is shown in Fig. S5 as "Exp. + lag 2". For Exp. + Gauss, a MLE approach for the total division time data is computationally complicated, so instead we chose the Method of Moments to fit the data in Fig. 3 (5). Alternatively, in this model it also makes sense to fit to the phases individually (exponential for G_1, Gaussian for $S/G_2/M$). We used a MLE approach to fit the two phases individually, and the results are shown in as "Exp. + Gaussian 2" in Fig. S5. Note that the fit to total division time is poorer compared with "Exp. + Gaussian", as expected, as this was not the goal of "Exp. + Gaussian 2". Note also that even though the phases are fit separately, the agreement between data and model is still poor due to a fundamental discrepancy between the shape of the distributions attempting to be fit and the actual data – there is a relatively flat initial phase in the G_1 data before a downturn that begins to look linear on a log scale (by contrast, an exponential is always linear passing through the origin, without a lag). It is a non-trivial feature of our data that the shape of the alpha curves for the individual phases are similar to the shape of the alpha-curve for total division time, consistent with stretched models (by contrast to compartment models where the shapes are distinctly different).

Confidence intervals for the model parameters were estimated with a bootstrap resampling procedure, whereby the data was resampled with replacement 1000 times and new best fits calculated. For the "Exp + Gaussian" model, the sample skewness can have a negative value. In this case, the method of moments used for fit fails (i.e., the sample does not resemble the suggested distribution), and parameter estimates obtained in these iterations were excluded from consideration. "Exp + Gaussian" parameter estimations failed in less than 6% of bootstrapping iterations for CpG B cells, 48% of cases for αCD40 B cells, 0% of cases for CD8+ T cells, and 5% of cases for OT-I cells.

Quality of fit can be visually assessed in Fig. 3, SI Fig. S5 and SI Fig. S6. Quantitative assessment was performed using the p-value of the two-sided Kolmogorov-Smirnov (KS) test as a measure of discrepancy between the observed empirical distribution and a model (SI Table S1, lower value means higher discrepancy). Note that although our time measurements are discrete (measured from video frame numbers), the models that we consider are based on continuous distributions. Furthermore, even in the case of discrete distributions the p-values can be used as a proxy measure for goodness-of-fit. The fits could be assessed using a likelihood based measure (e.g., Akaike information criterion). However, without a noise model, likelihoods can have zero values (e.g., in the lag-exponential model, empirical duration of $S/G_2/M$ is not constant). At the same time, addition of the noise model would unnecessarily involve extra parameters and assumptions.

SI Table S1. A summary of models and results of fitting to alpha plots as described in SI Text 1. For each estimated parameter, the table presents 95% confidence intervals obtained using bootstrapping with 1000 iterations.

Model / fitting method	**Parameter estimates / p-values of Kolmogorov-Smirnov test**					
Exp. + lag Duration of G_1 ($T_{div} - T_{grn}$) is exponentially distributed with parameter λ. Duration of $S/G_2/M$ (T_{grn}) is a constant t_0		λ, h^{-1}	t_0, h	G_1 p-value	$S/G_2/M$ p-value	Total p-value
	B cells, CpG	0.27 (0.21; 0.33)	8.47 (7.66; 9.10)	<0.00001	<0.00001	<0.00001
	B cells, αCD40	0.35 (0.22; 0.53)	8.86 (8.09; 9.80)	0.03700	0.00010	0.03310
	CD8+ T cells	0.25 (0.19; 0.35)	8.91 (8.12; 9.50)	<0.00001	<0.00001	0.00990

OT-I cells	0.66 (0.55; 0.76)	8.34 (8.14; 8.60)	<0.00001	<0.00001	<0.00001

Least squares regression to the logarithm of the empirical CDF of total division time (T_{div})

Exp. + Gaussian

Duration of G_1 is exponentially distributed with parameter λ. Duration of $S/G_2/M$ is independently normally distributed with parameters μ and σ

	λ, h^{-1}	μ, h	σ, h	G_1 p-value	$S/G_2/M$ p-value	Total p-value
B cells, CpG	0.38 (0.28; 1.07)	9.72 (8.59; 11.53)	2.28 (1.47; 3.03)	<0.00001	0.08864	0.90795
B cells, αCD40	2.99 (0.67; 2.42)	11.35 (9.21; 11.50)	2.07 (1.06; 2.19)	<0.00001	0.00269	0.63314
CD8+ T cells	0.32 (0.28; 0.42)	9.85 (8.97; 10.99)	2.06 (1.00; 3.01)	<0.00001	<0.00001	0.12662
OT-I cells	1.03 (0.72; 2.23)	9.16 (8.76; 9.71)	1.07 (0.80; 1.30)	<0.00001	<0.00001	0.77666

Method of moments

Stretched lognormal

Total division time is lognormally distributed with parameters μ and σ, and G_1 phase occupies proportion k_{G1} of the total division time

	k_{G1}	μ, h	σ, h	G_1 p-value	$S/G_2/M$ p-value	Total p-value
B cells, CpG	0.27 (0.24; 0.29)	12.34 (11.39; 13.37)	3.48 (2.74; 4.28)	0.27310	0.50390	0.80250
B cells, αCD40	0.22 (0.18; 0.26)	11.70 (10.74; 12.62)	2.16 (1.57; 2.56)	0.18060	0.20570	0.57020
CD8+ T cells	0.35 (0.33; 0.37)	12.95 (11.99; 13.91)	3.46 (2.59; 4.25)	0.00430	0.51860	0.07830
OT-I cells	0.28 (0.27; 0.29)	10.13 (9.89; 10.39)	1.43 (1.25; 1.61)	<0.00001	0.00250	0.84040

Maximum likelihood estimates; proportion k_{G1} is obtained from Fig. 2

Stretched Exp. + lag

Total division time is lag-exponentially distributed with exponential parameter λ and time lag t_0, and G_1 phase occupies proportion k_{G1} of the total division time

	k_{G1}	λ, h^{-1}	t_0, h	G_1 p-value	$S/G_2/M$ p-value	Total p-value
B cells, CpG	0.27 (0.24; 0.29)	0.27 (0.21; 0.33)	8.47 (7.66; 9.10)	<0.00001	<0.00001	<0.00001
B cells, αCD40	0.22 (0.18; 0.26)	0.35 (0.22; 0.53)	8.86 (8.09; 9.80)	<0.00001	0.01920	0.03310
CD8+ T cells	0.35 (0.33; 0.37)	0.25 (0.19; 0.35)	8.91 (8.12; 9.50)	<0.00001	<0.00001	0.00990
OT-I cells	0.28	0.66	8.34	<0.00001	<0.00001	<0.00001

	(0.27; 0.29)	(0.55; 0.76)	(8.14; 8.60)			

Least squares regression to the logarithm of the empirical CDF of total division time (T_{div}); proportion k_{G1} is obtained from Fig. 2

Stretched inverse Gaussian

Total division time follows an inverse Gaussian distribution with parameters λ and μ, and G_1 phase occupies proportion k_{G1} of the total division time

	k_{G1}	μ	λ	G_1 p-value	$S/G_2/M$ p-value	Total p-value
B cells, CpG	0.27 (0.24; 0.29)	12.33 (11.38; 13.36)	158.5 (116.02; 242.97)	0.27250	0.52590	0.80010
B, αCD40	0.22 (0.18; 0.26)	11.69 (10.74; 12.61)	367.0 (262.17; 658.71)	0.16600	0.21050	0.54740
CD8+ T cells	0.35 (0.33; 0.37)	12.97 (12.01; 13.91)	185.2 (142.79; 273.29)	0.00370	0.52990	0.07000
OT-I cells	0.28 (0.27; 0.29)	10.13 (9.89; 10.39)	512.7 (411.55; 672.43)	<0.00001	0.00390	0.84180

Maximum likelihood estimates; proportion k_{G1} is obtained from Fig. 2

Exp. + lag 2

Duration of G_1 ($T_{div} - T_{grn}$) is exponentially distributed with parameter λ. Duration of $S/G_2/M$ (T_{grn}) is a constant t_0.

Here $t_0 = \min(T_{div})$, and therefore an estimated parameter value usually coincides with the lower confidence bound.

	λ, h^{-1}	t_0, h	G_1 p-value	$S/G_2/M$ p-value	Total p-value
B cells, CpG	0.18 (0.15; 0.22)	6.70 (6.70; 7.60)	<0.00001	<0.00001	0.02760
B cells, αCD40	0.28 (0.24; 0.52)	8.17 (8.17; 9.67)	0.16110	<0.00001	0.46150
CD8+ T cells	0.21 (0.18; 0.28)	8.20 (8.20; 8.93)	<0.00001	<0.00001	0.17870
OT-I cells	0.32 (0.30; 0.41)	7.00 (7.00; 7.75)	<0.00001	<0.00001	<0.00001

Maximum likelihood estimates

Exp + Gaussian 2

Duration of G_1 is exponentially distributed with parameter λ. Duration of $S/G_2/M$ is independently normally distributed with parameters μ and σ

	λ, h^{-1}	μ, h	σ, h	G_1 p-value	$S/G_2/M$ p-value	Total p-value
B cells, CpG	0.30 (0.27; 0.33)	8.95 (8.20; 9.77)	2.90 (2.30; 3.44)	<0.00001	0.97190	0.76220
B cells, αCD40	0.38 (0.31; 0.47)	9.03 (8.12; 9.86)	1.93 (1.45; 2.23)	0.02150	0.45970	0.76860
CD8+ T cells	0.22 (0.20; 0.24)	8.45 (7.71; 9.15)	2.70 (2.15; 3.20)	<0.00001	0.21910	0.07180

OT-I cells	0.35 (0.33; 0.37)	7.30 (7.07; 7.54)	1.43 (1.23; 1.64)	<0.00001	0.25770	<0.00001

Independent maximum likelihood estimates for exponential and Gaussian parts

SI Text 2

FUCCI green accurately reports the onset of S phase. An important issue for the kinetic analysis of the cell cycle presented here is how faithfully the onset of green fluorescence (mAG-hGem) reports the onset of S phase for primary lymphocytes from the FUCCI reporter under the stimulation conditions used here. The experiments described in the main text and illustrated in SI Fig. S7 combining BrdU pulse labelling and direct staining of DNA with 7AAD allow us to address this issue too. A pulse of BrdU was added to the cultures of proliferating CpG-stimulated B cells for a brief time (15min), prior to fixation and detection with a fluorochrome-labelled antibody. Concurrently, DNA was stained with 7AAD. The flow cytometry plot of BrdU versus DNA (7AAD) in SI Fig. S7a separates the cells into various phases of the cell cycle (G_1, S, and G_2/M) as indicated by gates – G_1 cells have one copy of DNA and are not actively synthesising DNA (BrdU(-ve)), S cells are BrdU(+ve), and G_2/M cells have two copies of DNA and are BrdU(-ve). SI Fig. S7b shows the same cell-cycle populations but gated on BrdU versus FUCCI green instead of DNA. SI Fig. S7c demonstrates good correlation between the populations identified using these two alternative strategies. Importantly, the G_2/M populations are highly correlated, indicating that the FUCCI green(+ve) BrdU(-ve) population indeed corresponds to cells in G_2/M, not cells which have expressed FUCCI green prior to DNA synthesis. In fact, the BrdU(+ve) FUCCI green(-ve) cells in SI Fig. S7b indicate that cells do not express detectable green fluorescence prior to the onset of S phase. Finally, SI Fig. S7d shows that FUCCI green is comparable in sensitivity to DNA staining in detecting DNA synthesis.

SI Text 3

Mathematical modelling of BrdU pulse data. Our results indicate that the duration of S/G_2/M phase can be considered to be a fixed proportion of the total time to divide. Based on this premise, here we explore two further alternatives: a) the duration of S and G_2/M phases also stretch with the total division time; and b) the duration of S phase is constant.

The G_2/M phase is characterized by 2x level of DNA content and the absence of newly synthesized DNA. Therefore, when labelled with an instantaneous BrdU pulse and DNA stain (7AAD) cells in G_2/M stage are expected to form a BrdU(-) DNA(2x) subpopulation. However, with increased length of BrdU pulse, l, the proportion of cells remaining in this subpopulation, $p(l)$, decreases. This is because

some cells that were in G_2/M at the start of the pulse will divide and halve their DNA, becoming DNA(x1), while some cells in S phase at the start of the pulse will now be detected as BrdU(+ve).

We denote the total division time, T_{div}, the remaining time to next division, δ, and the time spent in the G_2/M phases of the cell cycle as T_{G2M}. The proportion of cells in a population that will fall into the BrdU(-) DNA(2x) subpopulation, $p(l)$, corresponds to those cells for which $0 \leq \delta \leq T_{G2M} - l$, i.e. those cells that were in G_2/M at the start of the pulse and have not exited that phase (divided) by the end. There are potentially many different approaches to calculating this proportion, however here we chose to base our analysis on previous work, combined with the additional stretching assumption.

We have previously shown that in a population of cells with times to divide following a known division-time distribution, $D(T_{div})$, in the absence of death, a steady state is reached where the distribution of cells $P_{ss}(\delta, T_{div})$ as a function of δ and T_{div} can be calculated(6). The formula for the steady-state distribution is as follows:

$$P_{ss}(\delta, T_{div}) = 2 \cdot c \cdot \exp(-c \cdot (T_{div} - \delta)) \cdot D(T_{div}), \qquad (1)$$

where c is constant defined as the solution to the following integral equation:

$$\int_0^\infty D(t) \cdot \exp(-c \cdot t) \cdot dt = \frac{1}{2}. \qquad (2)$$

See Eq. (0.9) in the Supplemental Information, and Eq. (3.10) in the main text of (6). Using these assumptions, the proportion $p(l)$ can be calculated as:

$$p(l) = \int_0^\infty \int_0^s P_{ss}(\delta, T_{div}) \cdot d\delta \cdot dT_{div}, \qquad (3)$$

where $s = \max(0, T_{G2M} - l)$. Based on our previous experience, a lognormal distribution is generally a good empirical choice for the division-time distribution, $D(\cdot)$(2, 3). Therefore, to fit to the BrdU pulse data, we first fit a lognormal distribution to the total division time data from the filming experiments reported in Fig. 3 under the same stimulation conditions. This gives us parameters for the mean and standard deviation of the lognormal distribution that are appropriate under those conditions, as shown in SI Table S2.

Recall that here we consider two alternatives: stretched S phase and constant S phase. Furthermore, note that stretched S phase implies stretched G_2/M phase. The simplest possible implementation of the stretched cell cycle model assumes $T_{G2M=}k_{G2M} \cdot T_{div}$, for each cell, where k_{G2M} is the proportion of total division time spent in G_2/M. Alternatively, S phase may take a constant time, T_S, in which case $T_{G2M} = k_{SG2M} \cdot T_{div} - T_S$, where k_{SG2M} is the stretching parameter for S/G_2/M derived from the filming data.

For the stretched S phase model, the only remaining free parameter in the above derivation is the stretching parameter, k_{G2M}. For the constant S phase model the only remaining free parameter is the S phase time, T_S. These parameters were optimised individually to fit each model to the observed data using numerical integration for the model, and residual sum of squares (RSS) as a goodness-of-

fit measure. We either performed an exhaustive search for these parameters (k_{G2M} between 0.01 and 1 with steps of 0.001, and T_S between 0 and 30 hours with 0.5 minutes steps), or used an optimization routine (MATLAB *fmincon* function with the default algorithm). In both cases, optimization converged to the same values for chosen precision. The full set of parameters and fitted values is reported in SI Table S2. Visually, stretched S model fits shown in Fig. 4c-d are reasonable, despite the simplicity of the model. There is some discrepancy between the data and model at later time points, which is more pronounced for the CD8+ T cell data. This discrepancy, while small in absolute terms, could be explained by more-sophisticated models where the full kinetics of the population are taken into account (as opposed to the simplifying assumptions of the model we used), or where the "stretching" parameter is allowed to vary slightly between cells.

SI Table S2. Full set of parameters used for fitting the models described in SI Text 3 to the data in Fig. 4c-d. Here μ and σ are the mean and standard deviation of the division-time distribution $D(\cdot)$, k_{SG2M} is the stretching parameter for S/G_2/M phase, and k_{G2M} is the stretching parameter for G_2M phase. The asterisks indicate fixed parameters: μ and σ are fixed by maximum likelihood estimation to the available data on total division time under the two conditions from the filming experiments, and k_{SG2M} is fixed to values obtained from Fig. 2. For each estimated parameter, the table presents 95% confidence intervals obtained using bootstrapping with 1000 iterations.

	μ, *h*	σ, *h*	k_{SG2M}	k_{G2M}	T_s, *h*	*RSS, stretched S*	*RSS, constant S*
B cells, CpG	12.34*	3.48*	0.73*	0.157 (0.155;0.159)	7.45 (7.40;7.49)	5.751	23.560
CD8+ T cells	12.95*	3.46*	0.65*	0.144 (0.142;0.147)	6.81 (6.77;6.86)	10.300	14.992

SI Text 4

Transition probability models are inconsistent with the FUCCI cell cycle filming data. In Fig. 3, S5 and S6 and in SI Text 1 we show that transition probability models based on Smith and Martin (1) do not fit our data from the FUCCI reporter well, assuming exact correspondence of the green phase (S/G_2/M) with the B phase of these models, and time prior to green (G_1) with A state. Here we show that even allowing for the transition in the model to occur some time before the FUCCI fluorescence transition (onset of S phase), as per the original Smith-Martin paper, there is still an inconsistency between transition probability models and two of our data sets.

Following the notation of the original paper(1), a transitional probability model divides the cell cycle into an *A* state and a *B* phase, such that the *A* state occurs within G_1 phase of the cell cycle, and the

B phase contains the S/G_2/M phases of the cell cycle (SI Fig. S9). The transition between the *A* state and the *B* phase need not necessary correspond exactly to the onset of *S* phase – it may occur earlier. Cells in *A* state are thought of as having a constant probability per unit time of exiting into *B* phase (analogous to radioactive decay), so that the distribution of time spent in *A* state is exponential. By contrast cells in *B* phase are thought of as being inexorably committed to cell division, which occurs after an orderly sequence of intracellular events taking a constant or near-constant time. The duration of *B* phase is usually represented as a constant (in the simplest implementation) or with a Gaussian random variable where the variance is implicitly assumed to be small and therefore makes little contribution to the variance in total division time(1, 7, 8). Another important aspect of a transition probability model is independence of durations of *A* state and *B* phase.

Let *a* and *b* denote the durations of *A* state and *B* phase, respectively, and let T_{div} denote the total duration of the cell cycle. In our experiments, for each cell, we measure the time of onset of green fluorescence, t_{grn}^{on}, which by definition occurs sometime after the transition from *A* state to *B* phase, and therefore divides *B* phase into two parts, b_1 and b_2 (note that b_2 is the same as T_{grn} used in the main text). In the following discussion *Cov* denotes covariance, *Var* denotes variance and *Std* denotes standard deviation, and overbars indicate sample estimates of population quantities. As in SI Text 1, because of the strong correlation in measured times for siblings we used data only for one randomly chosen sibling when calculating sample estimates.

We first estimate the relative contribution of the *B* phase to the variance of the total cycle duration T_{div}. We have

$$Var(b) = Var(b_1 + b_2) = Var(b_1) + Var(b_2) + 2 \cdot Cov(b_1, b_2). \qquad (4)$$

In our measurements (SI Table S3), for two of the datasets (CpG B cells and CD8+ T cells) we observe that

$$\overline{Cov(a + b_1, b_2)} \geq 0. \qquad (5)$$

At the same time, according to the transition probability model, the A state and B phase are independent, that is

$$Cov(a, b) = 0. \qquad (6)$$

Moreover, it seems reasonable to assume that the A state is independent of the two sub-phases, B_1 and B_2, that is

$$Cov(a, b_1) = Cov(a, b_2) = 0. \qquad (7)$$

Combined with Eq. (5), this means that for the transition probability model to be consistent with this data, we must have

$$Cov(b_1, b_2) \geq 0. \qquad (8)$$

Thus we have that

$$Var(b) \geq Var(b_2), \qquad (9)$$

$$\Rightarrow \frac{Std\,(b)}{Std\,(T_{div})} \geq \frac{Std\,(b_2)}{Std\,(T_{div})} \qquad (10)$$

In all of our datasets, the variance in b_2 is high relative to variance in total division time ($\overline{Std(b_2)}/\overline{Std(T_{div})}$ column). In the two datasets for which the above inequality (Eq. (10)) applies, this means that the relative contribution of the variance in *B* phase to variance in total division time is high, contrary to the idea of a constant or near-constant *B* phase.

Recall that in a transition probability model, a is exponentially distributed with mean μ_a (and standard deviation $\sigma_a = \mu_a$) and b is normally distributed with mean, μ_b, and standard deviation, σ_b. Measuring b_2 allows us to estimate an upper bound on the μ_a. Note that

$$Var(T) = Var(a) + Var(b_1) + Var(b_2) + 2 \cdot Cov(b_1, b_2), \qquad (11)$$

$$\Rightarrow Var(a) = Var(T) - Var(b_2) - (Var(b_1) + 2 \cdot Cov(b_1, b_2)). \qquad (12)$$

For the two datasets mentioned above, we have that

$$Var(b_1) + 2 \cdot Cov(b_1, b_2) \geq 0. \qquad (13)$$

Hence for these data,

$$Var(a) \leq Var(T_{div}) - Var(b_2), \qquad (14)$$

$$\Rightarrow \mu_a \leq \sqrt{Var(T_{div}) - Var(b_2)} \stackrel{\text{def}}{=} UB_a. \qquad (15)$$

We cannot measure μ_a directly, but we can estimate it as follows. In a transition probability model with exponentially and normally distributed parts, Exp. + Gaussian, the total duration of cell cycle, T_{div}, is an exponentially modified Gaussian (EMG) random variable(7), with three parameters, μ_a, μ_b, and σ_b. Using the method of moments, the parameters of an EMG distribution can be estimated based on the sample mean, $\bar{\mu}$, standard deviation, $\bar{\sigma}$, and skewness $\bar{y}$ of total division time (5). In particular the mean time of the exponential *A* state can be estimated as:

$$\overline{\mu_a} = \bar{\sigma} \cdot \left(\frac{\bar{y}}{3}\right)^{1/3}. \qquad (16)$$

On the other hand, we can also estimate the upper bound, UB_a, derived above (Eq. (15)) using our samples of T_{div} and b_2 times. As can be seen, in the two datasets for which the bound is valid the estimates are inconsistent (SI Table S3), which argues against the transition probability model being a good model for this data.

Again, we estimated 95% confidence intervals for these quantities using bootstrapping, i.e., fitting to the data sampled with replacement (in total 1000 iterations). The confidence intervals for UB_a and $\overline{\mu_a}$ overlap when calculated in this way, which could suggest that the violation of the inequality is not significant. However, we then went on to test the inequality for each bootstrap iteration. We

found that the inequality $\overline{\mu_a} \leq UB_a$ was satisfied in only 9% of iterations for CpG stimulated B cells, and 4% of iterations for CD8+ T cells, which favours the conclusion that the violation of the inequality is real. Note that, as explained in SI Text 1, with bootstrap resampling the sample skewness sometimes has a negative value, which is inconsistent with the EMG distribution, and therefore the Method of Moments fails and these bootstrap iterations are excluded from the analysis.

SI Table S3. Quantities calculated directly from our data and fitting of the Exp. + Gaussian transition probability model, as described in SI Text 4. Numbers in bold highlight inconsistency between our experimental results and a transition probability model. $\overline{UB_a}$ is left blank for the αCD40 B cell and OT-I T cell data because the bound is not valid for these data sets. For each estimated parameter, the table presents 95% confidence intervals obtained using bootstrapping with 1000 iterations.

Experiment	#cells	$\overline{Cov(a+b_1,b_2)}$, h^2	$\overline{Std(b_2)}$, h	$\overline{Std(T_{div})}$, h	$\frac{\overline{Std(b_2)}}{\overline{Std(T_{div})}}$	$\overline{UB_a}$, h	$\overline{\mu_a}$, h
B cells, CpG	49	0.9 (-0.53; 2.75)	2.93 (2.3; 3.44)	3.47 (2.63; 4.36)	0.85 (0.73; 1)	**1.85** (0.59; 2.85)	**2.61** (0.94; 3.63)
B, αCD40	17	-0.4 (-1.19; 0.42)	1.99 (1.48; 2.31)	2.09 (1.57; 2.46)	0.95 (0.75; 1.16)		0.33 (0.38; 1.48)
CD8+ T cells	56	1.58 (-0.64; 3.25)	2.73 (2.15; 3.19)	3.74 (2.81; 4.37)	0.73 (0.63; 0.88)	**2.56** (1.37; 3.25)	**3.12** (2.35; 3.58)
OT-I cells	143	-0.44 (-0.85; -0.11)	1.43 (1.22; 1.62)	1.44 (1.23; 1.65)	0.99 (0.91; 1.1)		0.97 (0.38; 1.35)

SI Text 5

Identification of microwells for manual annotation: Live cell microscopy was performed as described in Materials and Methods using imaging parameters listed in SI Table S4. Each recorded frame covers a number of square wells used to prevent cell migration outside the field of view. Since the number of wells is large, only potentially interesting wells (e.g., non-empty wells) were manually annotated. Candidate wells were selected for annotation using automatic division detection. The steps in this process are illustrated in SI Fig. S10a and described below.

Unless otherwise stated, all of the image processing was implemented using the software package Microgrid Array Tools (MATs) running under Matlab 2012a. Values of all the parameters listed below are shown in SI Table S5 for each experiment.

MATs has been released under GPLV3 and is available for download at:
https://github.com/johnfmarkham/mats

Camera DC offset

In the absence of light, each pixel takes a non-zero value. The first step in the process is to remove this. The average value was measured empirically and removed by subtracting the value in *CameraMeanBlackLevel.*

Correct for stage backlash

Due to wear on the motorised stage drive of the microscope there was some backlash which caused successive images not to be exactly aligned. This mis-alignment was corrected in software by finding the integer pixel offset that maximised correlation between successive transmission images and applying it to tall channels.

Uneven illumination correction

Each image was corrected for uneven illumination by using a correction image generated as follows: after the end of each experiment, images were taken of featureless areas away from the microwells with the microscope defocused. These were averaged over to remove any remaining position-dependent low frequency artefacts and the result smoothed by repeated application of a Gaussian kernel to remove any remaining high frequency noise.

Well detection

Microwells boundaries were detected using a range of heuristic methods applied to images from the transmission channel. The boundaries resulting putative boundaries were manually checked and corrected.

Background image generation

For each position, images representing the background were constructed as follows: for each channel the images were aligned spatially by using offsets determined by aligning the bright field images in a way which maximised the correlation between successive time points. After uneven illumination correction, the median value for each pixel in the aligned stack of images was then used as the overall median for that channel and position.

Thresholding for segmentation

For each image the corresponding background image was median-corrected and subtracted. The lowest *ProportionBackground* of pixels were taken to be background and set to zero.

Impulse noise removal

After thresholding, the remaining impulse noise was removed by application of a cellular automata filter. This method relies on the observation that impulse noise is not correlated in time, space or across channels, whereas the signal is. After thresholding, each non-zero pixel was set to zero if it did not have sufficient numbers of adjacent pixels that were also non-zero. The definition of *adjacent* has been generalised to mean (i) neighbouring pixels in the same frame and channel (of

which there are 8), (ii) pixels in the same position in the same channel in previous and following time points (of which there are 2) and (iii) in other channels (also 2 in this case). The minimum number of adjacent pixels needed to support a non-zero pixel is given by

MinimumNeighbours = *MinNeighboursSpace + MinNeighboursTime+ MinNeighboursChannel ,*

where the three quantities on the right hand side refer to (i), (ii) and (iii) above respectively.

Segmentation

The images after thresholding and impulse noise removal were smoothed to prevent over-segmentation using a Gaussian kernel generated with variance *SmoothingGaussianVariance* and width and height given by *SmoothingKernelSize*. Segmentation was done using the MATLAB *watershed()* function and segmented object properties were measured using the MATLAB *regionprops()* function. Segmented objects whose size fell outside the bounds set by [*MinAreaPixels*,*MaxAreaPixels*] and with eccentricity greater than *MaxEccentricity* or solidity less than *MinSolidity* were discarded.

Division Detection

The count of segmented objects in the mAG channel at each time point was used to locate wells likely to have started with one cell that then underwent two subsequent divisions to become four cells. Firstly, the count of segmented objects (putative cells) was smoothed by discarding a proportion of objects with the lowest fluorescence as given by *CutoffGFP* (SI Fig. S11a). The remaining counts (SI Fig. S11b) were put through a median filter of length *MedianFilterLength* time points (SI Fig. S11c). For a putative one-to-four cell well the resulting smoothed plot consisted of periods of time when the numbers of objects plateaued at one cell and then two cells, before subsequent divisions. These plateaus or "islands" sometimes had gaps that could be bridged (up to a maximum of *MaxMissingCellGap*). Often they had areas with extra objects due to oversegmentation that could be ignored (up to some proportion given by *MaxTwoCellInOneCellIsland* and *MaxThreeCellInTwoCellIsland*). The result consisted of regions that putatively contained either one or two cells (SI Fig. S11d). Physical constraints on the amount of time spent in $S/G_2/M$ were used to exclude wells where either of the extended islands fell outside the range [*MinGFPTime,MaxGFPTime*]. The remaining wells were then annotated.

Preparation of video for manual annotation: Those microwells identified for manual annotation were prepared using the steps shown in Fig. S10b. The steps which differ from the steps shown in Fig. S10a are described below.

Thresholding for annotation

Evenly illuminated fluorescence images were binarised for subsequent display and manual annotation. Pixel intensity quartiles, Q_1, Q_2 and Q_3 were computed for each image, and the intensity threshold value set at Q_1 + *ThresholdFactor* * (Q_3 - Q_2). This effectively set the threshold at some

value relative to the background fluorescence, and hence variations in illumination intensity were corrected for. The values for *ThresholdFactor* were chosen for each fluorescence channel separately in a way that minimised the number of false positives while maintaining acceptable sensitivity. The binarised image was then put through a median filter of radius one to remove pixel-based noise, such that a pixel's final value was determined by its eight nearest neighbours. This was found to be more effective at removing noisy pixels than application of the median filter followed by thresholding.

Encoding and display

Image sequences for each channel were encoded using the *ffdshow* Motion JPEG codec with one pass mode and quality set to 95. Transmission, false-coloured mAG and mKO2 channels, and an overlay channel where transmission and fluorescence channels were superimposed were displayed side-by-side for individual wells using automatically generated avisynth scripts in VirtualDub. Additionally, both thresholded (for annotation as above) and unthresholded versions were shown. Sample channel images are displayed in SI Fig. S12.

Manual scoring of movies: Putative one-cell wells that went on to become four-cell wells were selected for manual annotation based on the heuristic described above. By inspecting the bright field channel for morphological changes, the frame at which the two daughter cells came into existence was marked as the beginning of the annotation process, and the frame number recorded. Sister cells were then tracked by size, relative positions, presence and amount of fluorescence, morphology and granularity.

Using the overlay as a reference, the binarised fluorescence channels were inspected until specks of colour appeared. Occasionally the colour flickered on and off, so the unthresholded (but uneven illumination-corrected) images were used as a reference to rule out any noise that passed the threshold. The first frame at which cells became fluorescent was recorded for each channel.

Annotations continued until each cell divided, died, or was lost and could no longer be tracked. Division was recorded as the frame closest to the completion of cytokinesis, and death at the beginning of blebbing or membrane rupture. Losses were infrequent and either due to the inability to distinguish between neighbouring cells, or motile cells departed from the microwell. Tracking became increasingly difficult with more divisions due to increased number of cells, clumping and cell movement, but the cells that remained alive would often divide multiple times over the duration of the experiment.

SI Table S4. Imaging parameters.

	B cells, CpG	B cells, αCD40	CD8+ T cells	OT-I T cells
min/frame	3	10	4	10

	positions	28	144	44	104
	total images/second	0.78	1.20	0.73	0.87
	channels	5	5	4	5
	wells/pos	20	48	48	48
	wells	560	6,912	2,112	4,992
	time points	1,781	395	1,040	490
	time (hours)	89	66	69	82
	images	249,340	284,400	183,040	254,800
	data (TB)	0.48	0.54	0.35	0.49
	data points (auto)	44	216	112	510
mKO2	**Filter Set**	Zeiss 45	Semrock GFP/DsRed-A	Semrock GFP/DsRed-A	Semrock GFP/DsRed-A
	Excitation Intensity (%)	100	25	100	100
	Exposure (ms)	250	100	250	250
mAG	**Filter Set**	Zeiss 13	Semrock GFP/DsRed-A	Semrock GFP/DsRed-A	Semrock GFP/DsRed-A
	Excitation Intensity (%)	25	15	25	25
	Exposure (ms)	250	100	250	250

SI Table S5. Imaging processing parameters.

		B cells, CpG	**B cells, αCD40**	**CD8+ T cells**	**OT-I T cells**
Camera DC Offset	*CameraMeanBlackLevel*	32	32	32	32
Thresholding for segmentation	*ProportionBackground*	0.95	0.95	0.95	0.95
Impulse noise removal	*MinNeighboursSpace*	4	4	4	4
	MinNeighboursTime	2	2	2	2
	MinNeighboursChannel	1	1	1	1
Segmentation	*SmoothingKernelSize (pixels)*	11	11	11	11
	SmoothingGaussianVariance (pixels)	10	10	10	10
	MinAreaPixels (pixels)	20	20	20	20
	MaxAreaPixels(pixels)	1600	1600	1600	1600
	MaxEccentricity	0.8	0.7	0.7	0.8
	MinSolidity	0.5	0.5	0.5	0.5
Division detection	*MedianFilterLength (frames)*	11	8	8	11
	CutoffGFP	0.05	0.05	0.8	0.05
	MaxMissingCellGap (frames)	1	1	2	1
	MinGFPTime (hours)	1	1	1	0.1

	MaxGFPTime (hours)	25	25	25	25
	MaxTwoCellInOneCellIsland	0.2	0.1	0.2	0.1
	MaxThreeCellInTwoCellIsland	0.2	0.1	0.2	0.1
	PercentileFilter	0.5	0.75	0.75	0.5
Thresholding for annotation	*ThresholdFactor (mAG, mKO2)*	(1.3, 0.8)	(1.3, 0.8)	(1.3, 0.8)	(1.3, 0.8)

SI Text 6

In Figure 3 (alpha plots), data points below 0.01 are not shown due to space limitations. These are 1 to 3 points per plot. The points that were omitted are listed below. Note that these points were accounted for in numerical analyses described in this work.

SI Table S6. List of points not shown in Figure 3. Points are presented in the (x; y) format.

	G_1 ($T_{div} - T_{grn}$)	$S/G_2/M$ (T_{grn})	Total (T_{div})
B cells, CpG	(8.3000; 0)	(16.1000; 0)	(24.4000; 0)
B cells, αCD40	(5.8333; 0)	(16.8334; 0)	(18.1667; 0)
CD8+ T cells	(9.4667; 0.0088) (10.6667; 0)	(16.8000; 0.0088) (17.0667; 0)	(23.2000; 0.0088) (23.4667; 0)
OT-I cells	(5.8333; 0.0070) (7.1667; 0.0035) (9.3333; 0)	(10.3333; 0.0070) (12.0000; 0.0035) (13.1667 0)	(14.0000; 0.0070) (16.1667; 0.0035) (17.1667; 0)

References

1. Smith JA & Martin L (1973) Do Cells Cycle? *Proc Natl Acad Sci USA* 70(4):1263-1267.
2. Duffy K, *et al.* (2012) Activation-Induced B Cell Fates Are Selected by Intracellular Stochastic Competition. *Science* 335(6066):338--341.
3. Hawkins ED, Markham JF, McGuinness LP, & Hodgkin PD (2009) A Single-Cell Pedigree Analysis of Alternative Stochastic Lymphocyte Fates. *Proc Natl Acad Sci USA* 106(32):13457-13462.
4. Castor LN (1980) A G1 Rate Model Accounts for Cell-Cycle Kinetics Attributed to 'Transition Probability'. *Nature* 287(5785):857-859.
5. Olivier J & Norberg MM (2010) Positively Skewed Data: Revisiting the Box-Cox Power Transformation. *International Journal of Psychological Research* 3(1):69-78.
6. Dowling MR, Milutinović D, & Hodgkin PD (2005) Modelling Cell Lifespan and Proliferation: Is Likelihood to Die or to Divide Independent of Age? *Journal of the Royal Society: Interface* 2(5):517--526.
7. Golubev A (2010) Exponentially Modified Gaussian (EMG) Relevance to Distributions Related to Cell Proliferation and Differentiation. *Journal of Theoretical Biology* 262(2):257-266.
8. Golubev A (2012) Transition Probability in Cell Proliferation, Stochasticity in Cell Differentiation, and the Restriction Point of the Cell Cycle in One Package. *Progress in Biophysics and Molecular Biology* 110(1):87-96.

Figures

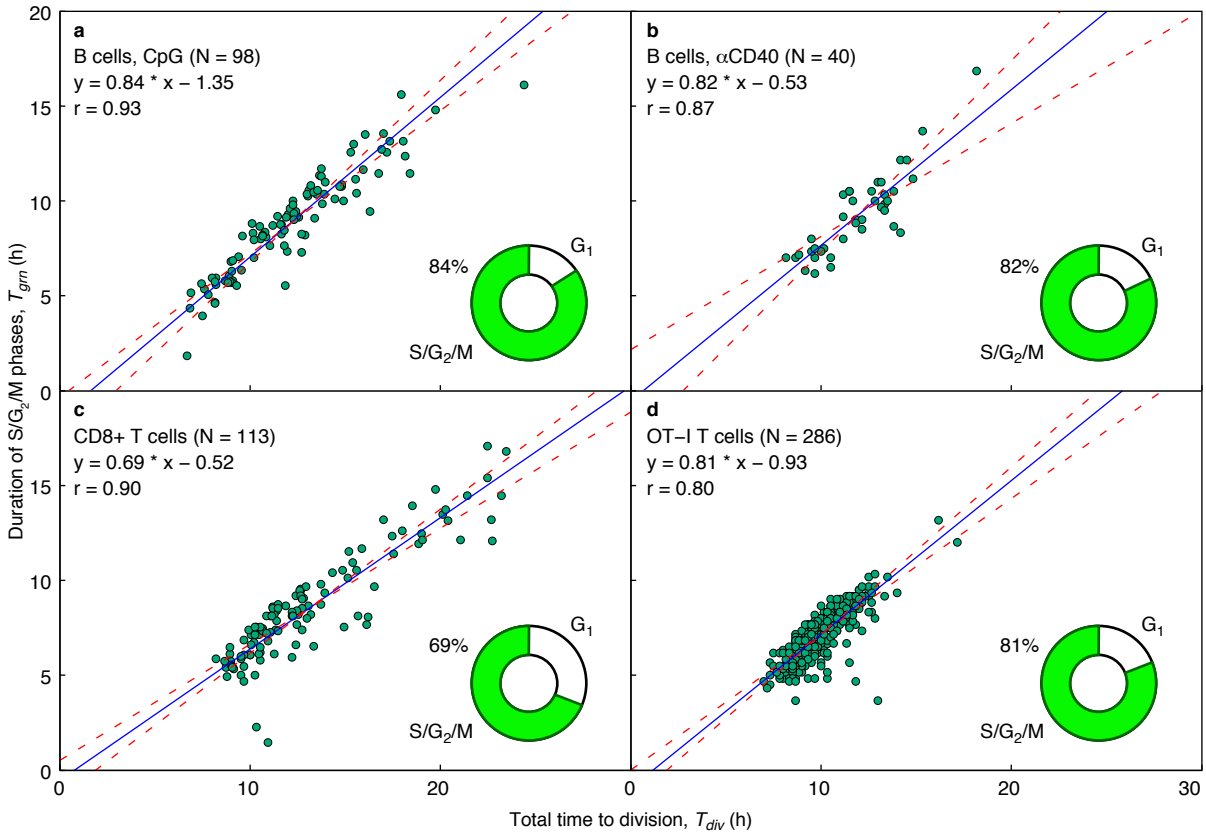

SI Fig. S1 | Linear relationship between the total division time and the duration of the combined S/G_2/M phases for primary B- and T-lymphocytes responding to different stimuli. Data from Fig. 2 was permitted to have linear fits with a non-zero intercept. **(a)** CpG stimulated B cells, slope = 0.84 (0.76;0.96), intercept = -1.35 (-2.73;-0.34), r = 0.93 (0.90;0.95). **(b)** αCD40 and IL-4 stimulated B cells, slope = 0.82 (0.60;1.01), intercept = -0.53 (-2.75;1.82), r = 0.87 (0.77;0.93). **(c)** αCD3 and IL-2 stimulated CD8+ T cells, slope = 0.69 (0.61;0.76), intercept = -0.52 (-1.46;0.35), r = 0.90 (0.86;0.93). **(d)** OT-I CD8+ T cells stimulated with high affinity peptide and IL-2, slope = 0.81 (0.72;0.88), intercept = -0.93 (-1.72;-0.05), r = 0.80 (0.76;0.84). Solid blue lines show the fitted linear relations of the form y = (slope)*x + (intercept); dashed red lines (and numbers in brackets) show 95% bootstrapped confidence intervals; r and numbers in brackets show Pearson's correlation coefficient and 95% confidence intervals based on Fisher transformation. The confidence intervals either cover the origin or pass close to the origin, suggesting that a simpler model without an intercept can give a reasonable explanation of the data (as presented in Fig. 2).

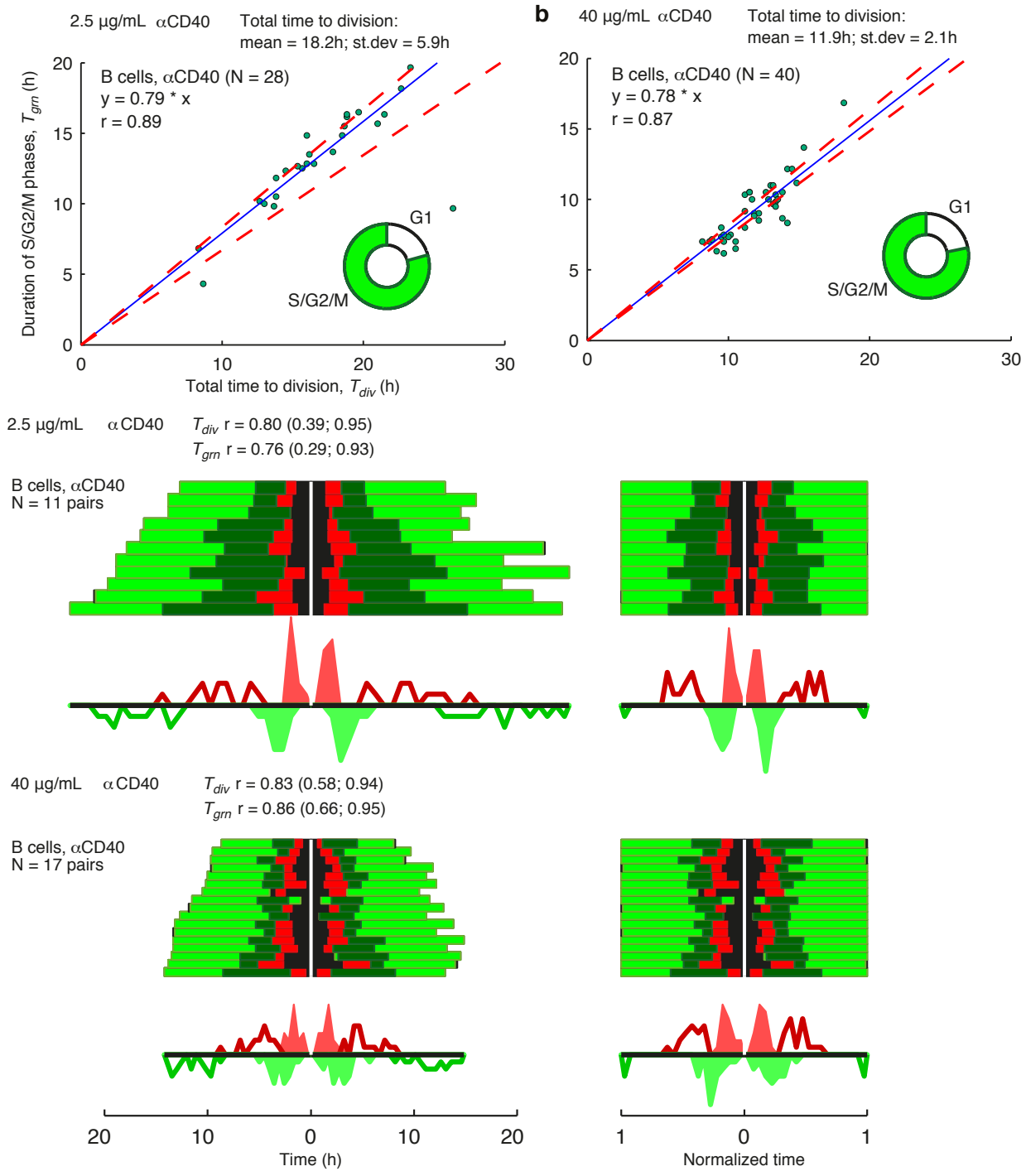

SI Fig. S2 | Linear relation and sibling correlations are preserved in a slowly dividing population. B cells stimulated with IL-4 and 2.5 µg/mL of αCD40 **(a,c)** or 40 µg/mL of αCD40 **(b,d)**. **(a)** slope = 0.79 (0.67;0.84), r = 0.89 (0.77;0.95). **(b)** slope = 0.78 (0.74;0.82), r = 0.87 (0.77;0.93). Solid blue lines show the fitted linear relations of the form y = (slope)*x; dashed red lines show 95% bootstrapped confidence intervals; r is Pearson's correlation coefficient and

numbers in brackets below show 95% confidence intervals based on Fisher transformation. The duration of the combined $S/G_2/M$ phases (estimated as the duration of green fluorescence) appears to take approximately the same proportion (slope of the fitted line, k_{SG2M}) of the total division time within each group of cells. This proportion is schematically represented with pie charts. **(c,d)** Bars represent total times to divide for sibling cells (left and right hand sides), and colours show temporal location of red fluorescence (red), green fluorescence (green), both (dark green) or none (black). The durations are shown either in hours (left) or relative to the total time to divide (right). The histograms under each group of bars show the distributions of times to onset of red (filled red curves), offset of red (red lines), onset of green (filled green curves), offset of green (green lines) for corresponding groups of cells. Here, r and numbers in brackets show Pearson's correlation coefficient and 95% confidence intervals based on Fisher transformation for the total division time (T_{div}) or duration of green fluorescence (T_{grn}) for sibling cells.

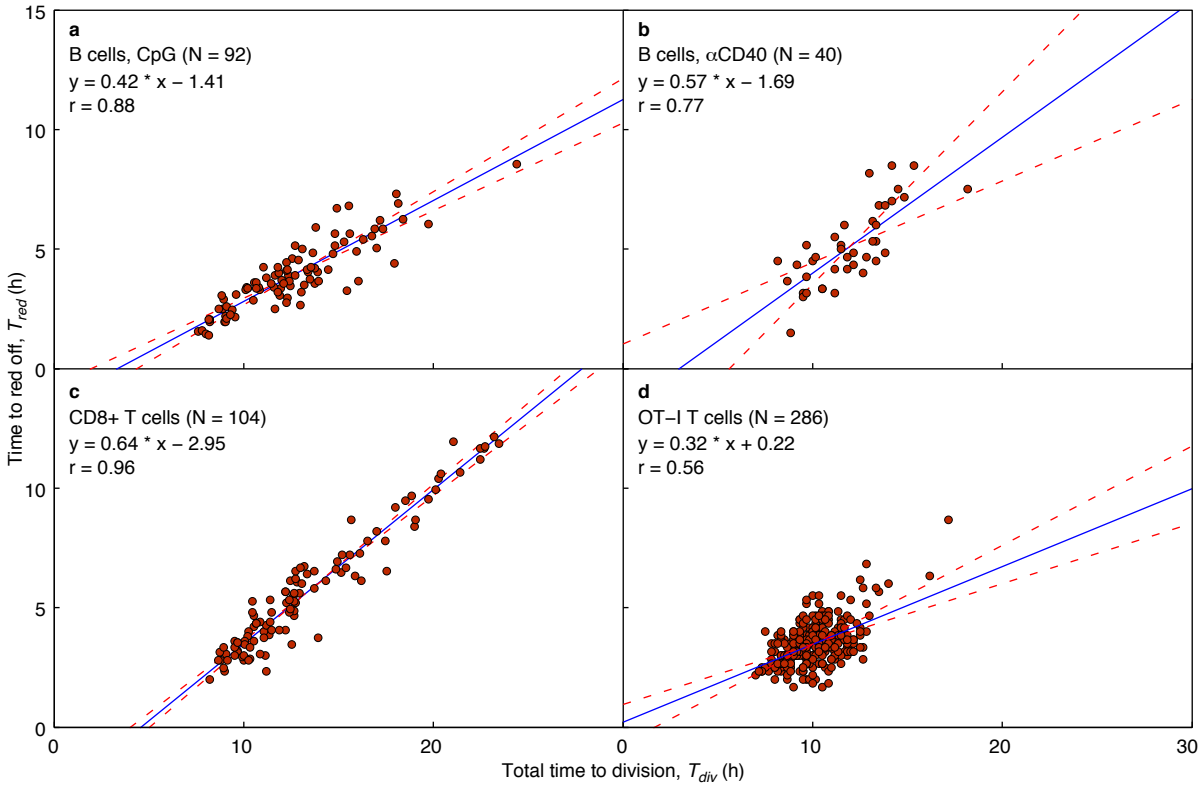

SI Fig. S3 | Linear relationship between the total division time and the time to offset of red fluorescence for primary B- and T-lymphocytes responding to different stimuli. (a) CpG stimulated B cells, slope = 0.42 (0.37;0.47), intercept = -1.41 (-1.92;-0.75), r = 0.88 (0.83;0.92). **(b)** αCD40 and IL-4 stimulated B cells, slope = 0.57 (0.34;0.80), intercept = -1.69 (-4.46;0.94), r = 0.77 (0.61;0.87). **(c)** αCD3 and IL-2 stimulated CD8+ T cells, slope = 0.64 (0.61;0.68), intercept = -2.95 (-3.39;-2.47), r = 0.96 (0.95;0.98). **(d)** OT-I CD8+ T cells stimulated with high affinity peptide and IL-2, slope = 0.32 (0.25;0.42), intercept = 0.22 (-0.64;0.91), r = 0.56 (0.48;0.64). Solid blue lines show the fitted linear relations of the form y = (slope)*x + (intercept); dashed red lines (and numbers in brackets) show 95% bootstrapped confidence intervals; r and numbers in brackets show Pearson's correlation coefficient and 95% confidence intervals based on Fisher transformation. The signal to noise ratio was lower for red fluorescence than for green fluorescence and there is more noise in the data.

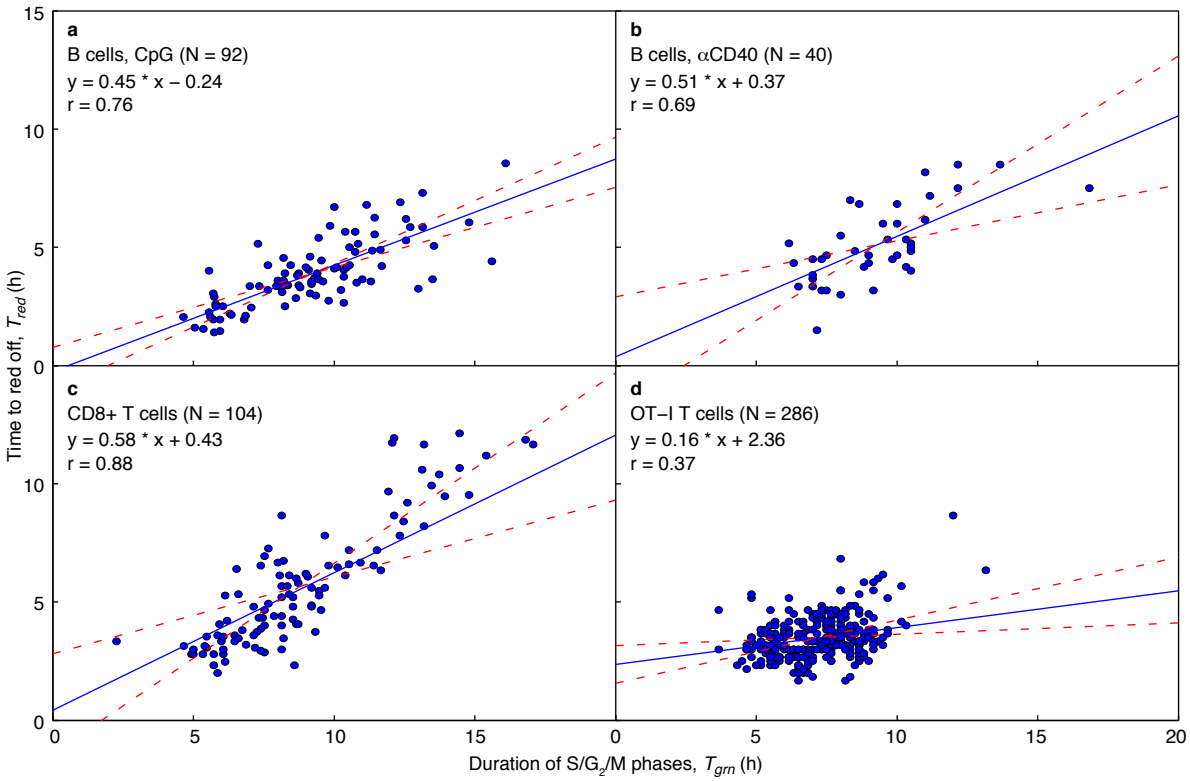

SI Fig. S4 | Linear relationship between the duration of S/G_2/M phases and the time to offset of red fluorescence for primary B- and T-lymphocytes responding to different stimuli. (a) CpG stimulated B cells, slope = 0.45 (0.34;0.54), intercept = -0.24 (-0.97;0.70), r = 0.76 (0.65;0.83). **(b)** αCD40 and IL-4 stimulated B cells, slope = 0.51 (0.24;0.74), intercept = 0.37 (-1.80;2.72), r = 0.69 (0.48;0.82). **(c)** αCD3 and IL-2 stimulated CD8+ T cells, slope = 0.58 (0.32;0.80), intercept = 0.43 (-1.41;2.12), r = 0.88 (0.82;0.92). **(d)** OT-I CD8+ T cells stimulated with high affinity peptide and IL-2, slope = 0.16 (0.05;0.27), intercept = 2.36 (1.59;3.15), r = 0.37 (0.26;0.46). Solid blue lines show the fitted linear relations of the form y = (slope)*x + (intercept); dashed red lines (and numbers in brackets) show 95% bootstrapped confidence intervals; r and numbers in brackets show Pearson's correlation coefficient and 95% confidence intervals based on Fisher transformation. There is a statistically significant correlation in all four cases, although it is only mild in the case of OT-I cells.

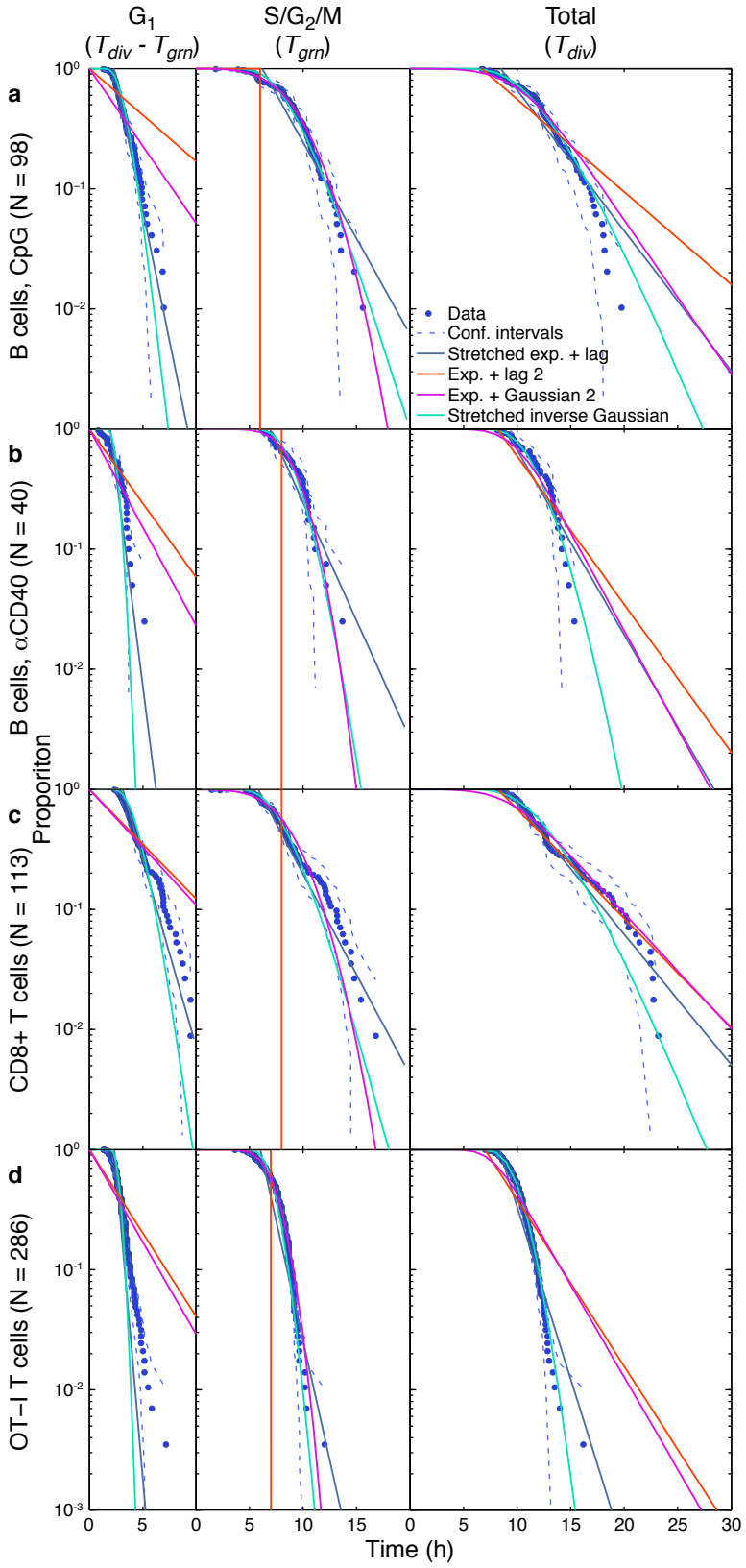

SI Fig. S5 | Alpha plots (empirical tail distributions) for estimated times spent in G_1 phase (left column), $S/G_2/M$ phases (middle column) and total division times (right column)

overlaid with fitted models for different experiments. (a) CpG stimulated B cells, **(b)** αCD40 and IL-4 stimulated B cells, **(c)** αCD3 and IL-2 stimulated CD8+ T cells, **(d)** OT-I CD8+ T cells stimulated with high affinity peptide and IL-2. Lag-exponential, exponentially modified Gaussian (Smith and Martin model), stretched lag-exponential and stretched inverse Gaussian models were defined and fitted as explained in SI Text 1.

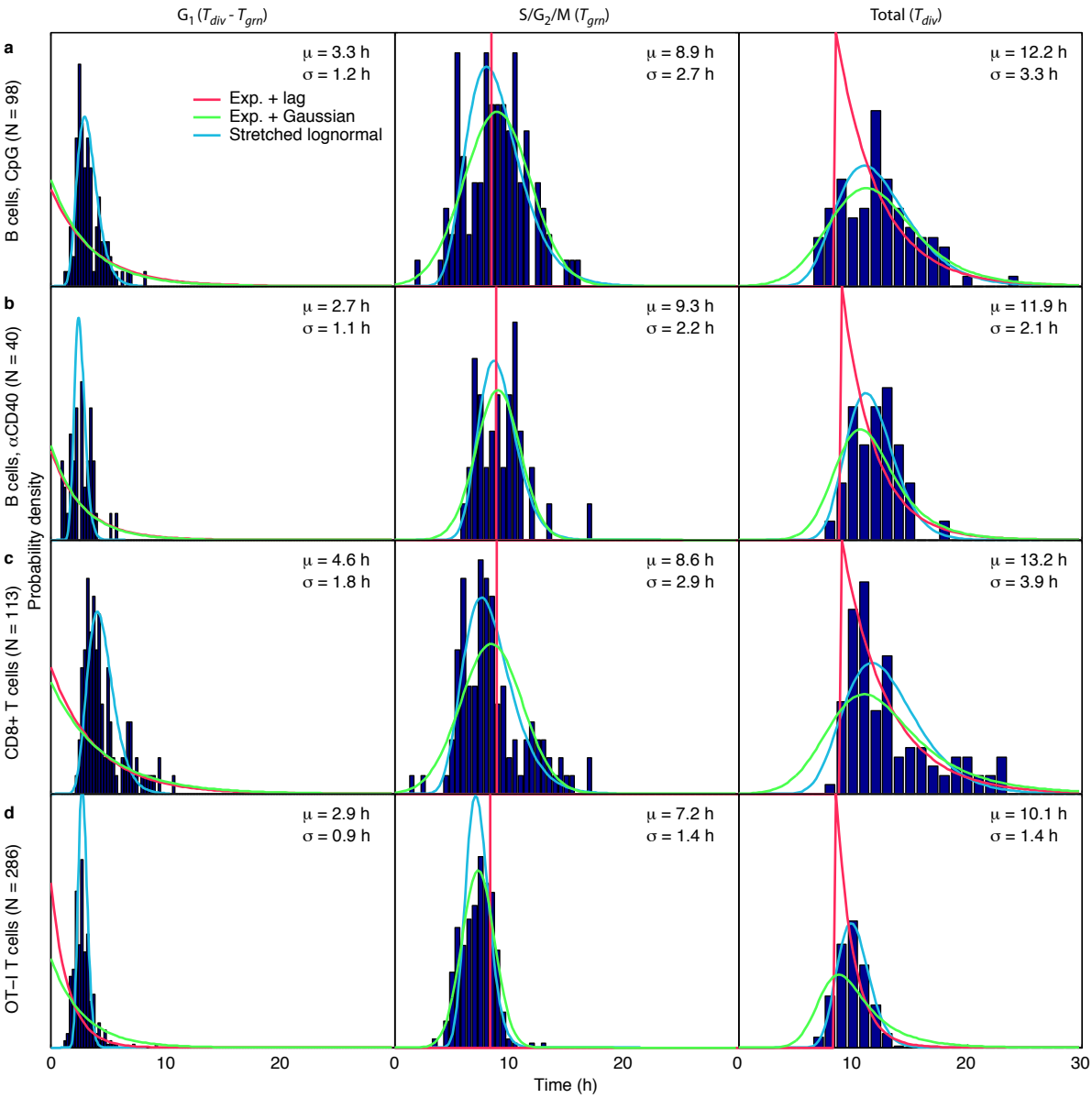

SI Fig. S6 | Histograms for estimated times spent in G_1 phase (left column), $S/G_2/M$ phases (middle column) and total division times (right column) overlaid with fitted models for different experiments. (a) CpG stimulated B cells, **(b)** αCD40 and IL-4 stimulated B cells, **(c)** αCD3 and IL-2 stimulated CD8+ T cells, **(d)** OT-I CD8+ T cells stimulated with high affinity peptide and IL-2. Here μ and σ denote respectively sample mean and standard deviation. In all cases the standard deviation in S/G2/M time is comparable to the standard deviations in total division time, as suggested by Fig. 2. Lag-exponential, exponentially modified Gaussian (Smith and Martin model) and stretched lognormal models were defined and fitted as explained in SI Text 1. The histograms are binned in 15 minute (left column), 30 minute (middle column) or 1 hour (right column) intervals, and the counts are normalized by the total histogram area.

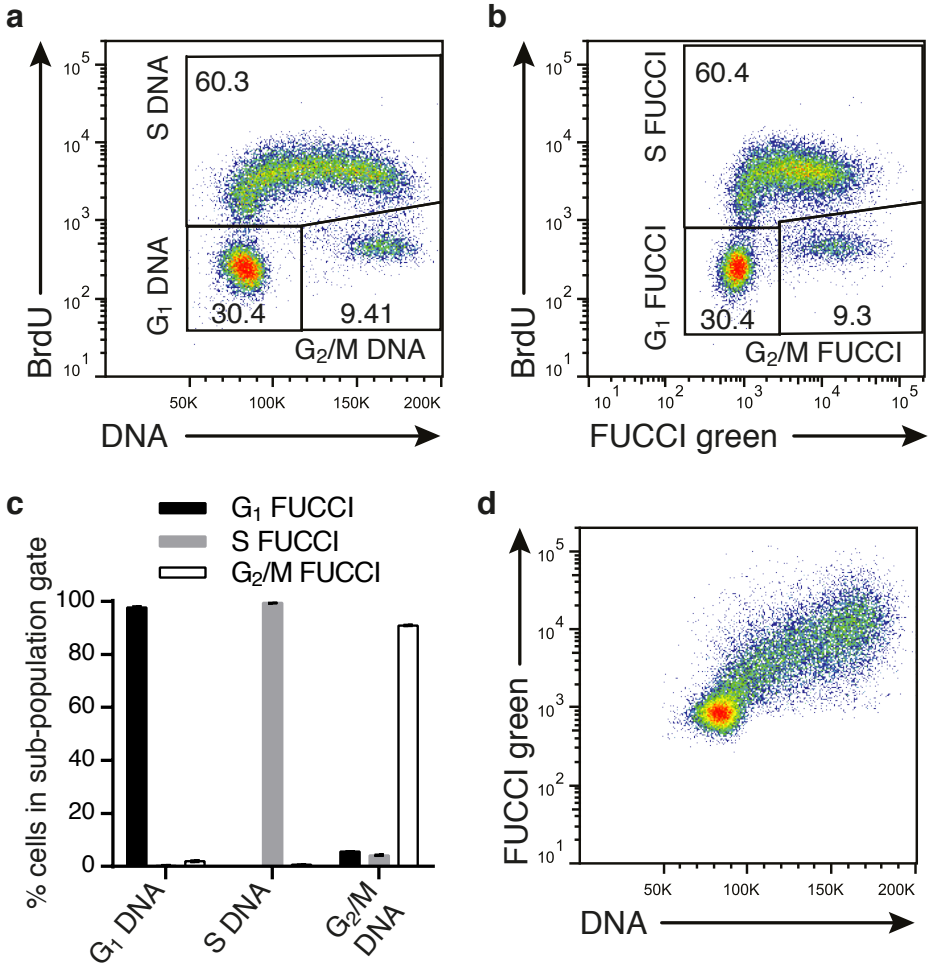

SI Fig. S7 | DNA labelling with BrdU and direct staining with 7AAD in proliferating FUCCI lymphocytes for separating G_1, S, and G_2/M cells by flow cytometry. a–d, Flow cytometric analysis of CpG-stimulated B cells pulsed with BrdU for 15 min. **(a)** This short BrdU pulse allows the separation of cells into different cell cycle phases in the BrdU versus DNA plot. **(b)** Visually similar to **a**, the BrdU versus FUCCI green plot also allows gating into different cell cycle phases. **(c)** Each sub-population from **a** (G_1-DNA, S-DNA or G_2/M-DNA) was individually assessed for its distribution across the BrdU versus FUCCI green sub-populations (G_1-FUCCI, S-FUCCI or G_2/M-FUCCI) in **b**. High concordances between corresponding sub-populations confirm that the gates identified by BrdU versus either DNA or FUCCI green are essentially the same cell populations. **(d)** The FUCCI green versus DNA plot shows that they are equally sensitive for detecting cells that have begun DNA synthesis.

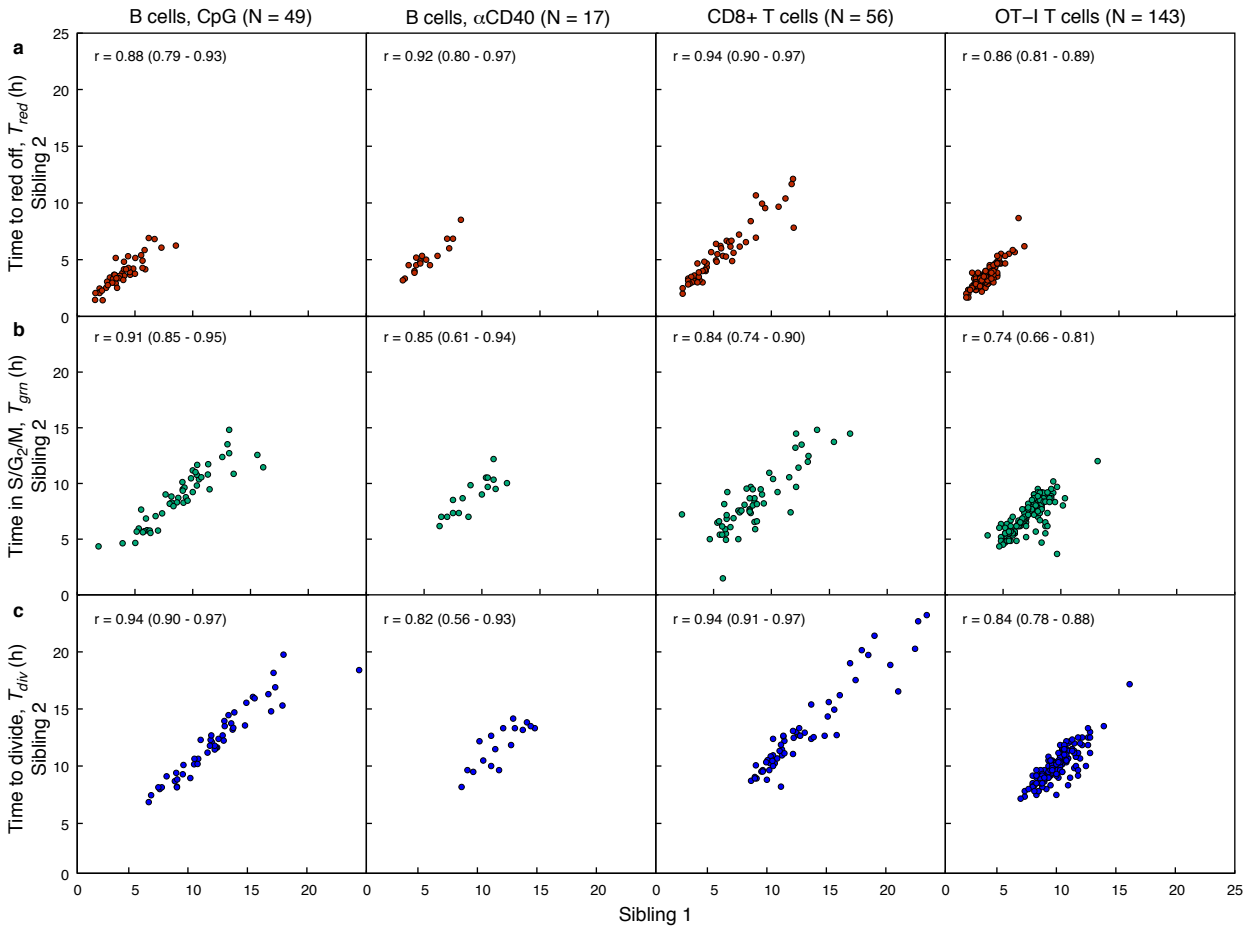

SI Fig. S8 | Scatter plots of estimated times for sibling cells. There is a strong correlation in time to offset of red fluorescence **(a)**, combined $S/G_2/M$ phase **(b)** and total division times **(c)** for sibling cells in each experiment. Here, r and numbers in brackets show Pearson's correlation coefficient and 95% confidence intervals based on Fisher transformation.

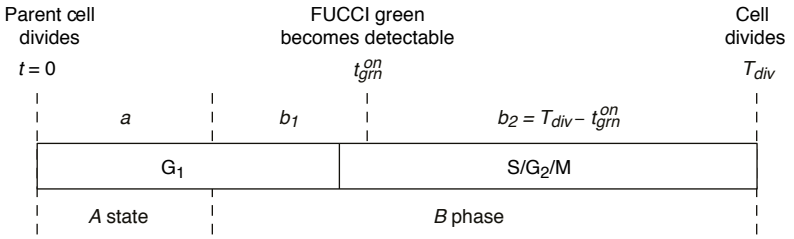

SI Fig. S9 | A transition-probability model where cell cycle is divided into independent parts – A state and B phase. In our experiments the onset of green fluorescence, t_{grn}^{on}, divides the *B* phase into two parts, b_1 prior to the onset, and b_2 after onset. In the figure, *A* state is aligned with G_1 for visual clarity. However, *A* state can start anywhere as long as it is contained entirely within G_1, and in some cases, b_1 can comprise a sum of two discontinuous parts. This does not affect the argument in SI Text 4.

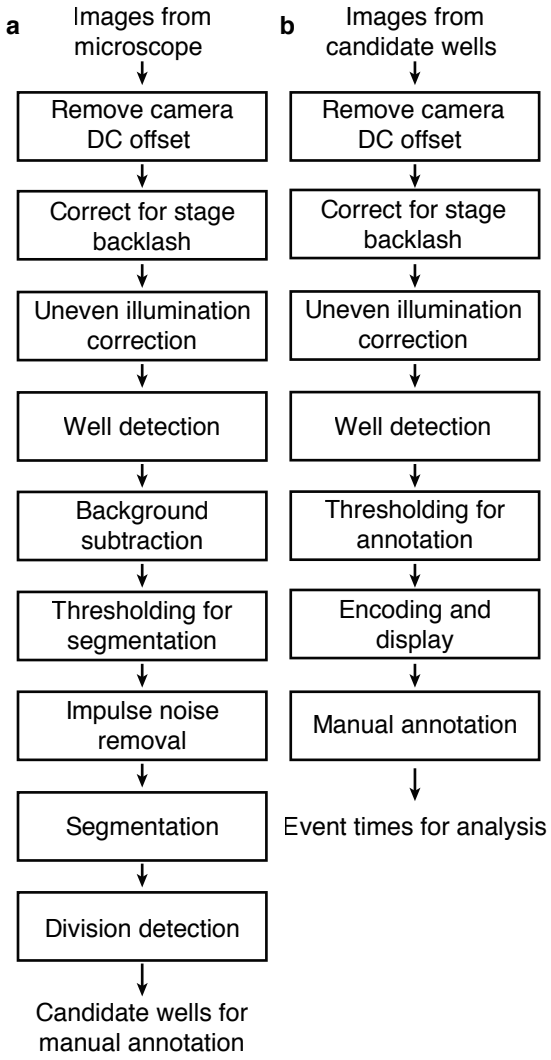

SI Fig. S10 | Work flow of image processing. (a) Raw TIFF images from the microscope were processed by a pipeline to identify candidate wells for annotation. **(b)** Images for the candidate wells were converted into movies that were manually annotated.

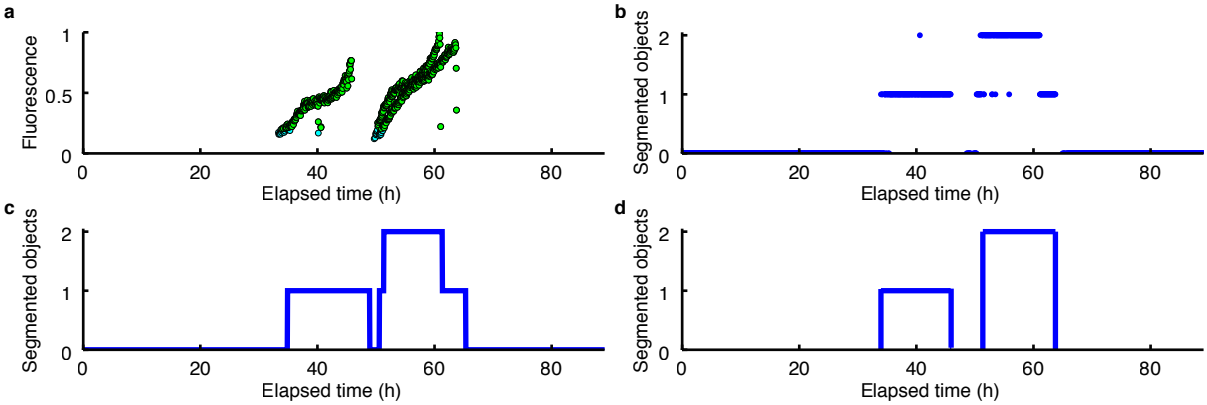

SI Fig. S11 | Automatic detection of cell division was used to select wells for annotation. **(a)** mAG (green) fluorescence versus time for segmented objects. **(b)** The lowest values (cyan in **a**) were discarded while the remainder (green in **a**) were used to produce putative cell counts. **(c)** Noise was removed by application of a median filter. For wells of interest, regions with one or two cells appeared as 'islands'. **(d)** Further noise was corrected for to produce the final putative one and two cell regions.

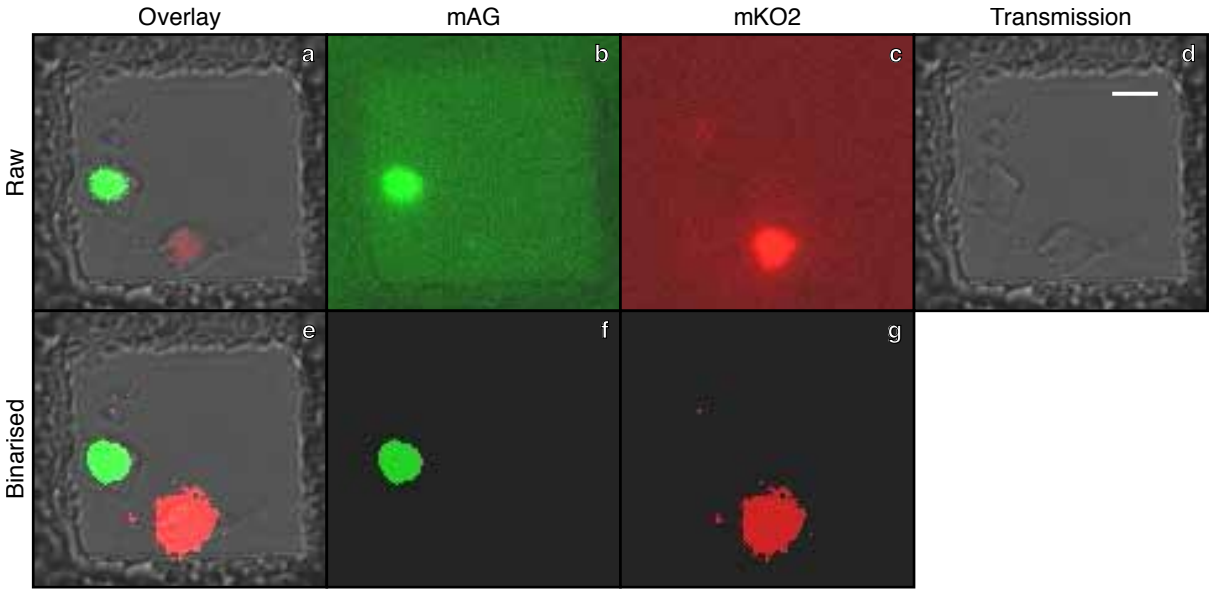

SI Fig. S12 | Display of movies for manual annotation. (a) Transmission image overlaid with thresholded versions of mAG and mKO2 channels. **(b)** Unthresholded mAG channel. **(c)** Unthresholded mKO2 channel. **(d)** Transmission channel. **(e)** Transmission image overlaid with binarised versions of mAG and mKO2 channels. **(f)** Binarised mAG channel. **(g)** Binarised mKO2 channel.